THESIS FOR THE DEGREE OF LICENTIATE OF ENGINEERING

Flow dynamics of complex fluids: characterization, modeling and flow in milifluidic channel

Ases Akas Mishra

CHALMERS
UNIVERSITY OF TECHNOLOGY

Department of Industrial and materials science
Chalmers University of Technology
Gothenburg, Sweden, 2023

Flow dynamics of complex fluids: characterization, modeling and flow in milifluidic channel

Ases Akas Mishra

Technical Report No. IMS-2023-5
This thesis has been prepared using LaTeX.

Department of Industrial and materials science
Chalmers University of Technology
SE-412 96 Gothenburg, Sweden
Phone: +46 (0)31 772 1000
www.chalmers.se

Printed by Chalmers Reproservice
Gothenburg, Sweden, May 2023

Dedicated to the memory of Fredrik Innings (1966-2022)

Abstract

Complex fluids are used in a wide range of applications in biomedical, food, cosmetic, chemical and pharmaceutical industries. Their complex material behaviour arises primarily from their rheological properties and is complimented by factors such as their multi-phase nature, biological component and complex microstructure. A comprehensive understanding of the material rheology is crucial to studying the flow dynamics of these complex fluids in industrial flow configurations. Additionally, to improve and ensure their consistent and efficient production and processing, prediction of their flow properties is of utmost importance. This necessitates the use of non-linear rheological constitutive models that can predict the material response during flow. In this framework, the PhD project aims at improved material characterization of the rheological properties of thixo-elasto-viscoplastic (TEVP) fluids, studying their flow dynamics in various flow configurations and prediction thereafter. In this thesis, three widely used complex fluids, yogurt, Carbopol and Laponite, were studied and their viscoelastic, viscoplastic and thixotropic material responses were extensively characterized. Numerical modeling was performed to predict the thixotropic behaviour of yogurt in Multi interval thixotropic tests (MITT), by curve fitting four phenomenological thixotropic models to hysteresis loop tests. The numerical modeling results show promising predictive capabilities and form the ground work required for flow simulations. This was followed by a microstructural study to investigate the effect of thixotropic material behaviour on the structural evolution of the material. To study the flow dynamics, a non-intrusive optical based imaging solution was developed using the Doppler-optical coherence tomography method to visualize the flow field of complex fluids in milifluidic channels for the first time. Different types/concentrations/structural states of the fluids were considered to investigate the effects of the rheological material functions on the flow field. An ex-situ rheometric method was developed and used to construct the shear stress distribution map inside the channel, which provided useful insights into the structural changes occurring as a result of the competition between the materials' flow and rheological properties. Results obtained from this study will be used to construct and validate simulation models in the future.

Keywords: Rheology, complex fluids, numerical modeling, milifluidic channel, flow visualization.

List of Publications

This thesis is based on the following publications:

[A] **Ases Akas Mishra**, Viney Ghai, Dragana Arlov, Fredrik Innings, Roland Kádár, "Structural kinetic modeling of yogurt thixotropy and predictability thereof in simple shear".
Manuscript submitted.

[B] **Ases Akas Mishra**, Kasra Amini, Amit Kumar Sivakumar, Dragana Arlov, Fredrik Innings, Roland Kádár, Outi Tammisola, Fredrik Lundell, "Velocity field assessment of thixo-elasto-viscoplastic fluids in a milifluidic channel with Doppler-OCT".
Manuscript.

Acknowledgments

I extend my sincere gratitude to my PhD advisor and mentor at Chalmers University of Technology, Prof. Roland Kádár for his guidance and encouragement. Thank you for believing in my ideas and helping me push my boundaries to always deliver the highest quality of scientific work.

I would like to thank my co-supervisor from TetraPak Dr. Dragana Arlov for motivating and helping me to work towards solving problems of industrial relevance. Thank you for always asking the difficult fundamental questions that make me work harder to solve, and learn a lot in the process.

I would take this opportunity to remember late Dr. Fredrik Innings, who in the short period while he was my co-supervisor, taught me to go back to the fundamentals when faced with a challenging problem in research.

My journey so far in academia and research has been full of joyous moments, thanks to my wonderful team mates and collaborators from the Rheology and Processing of Soft matter lab. I thank you for your support and for wonderful technical discussions we have had.

A special thanks to Amit Sivakumar for his invaluable help with experiments.

Last but not the least, I am grateful to my family and friends who have always encouraged and supported me to aim higher and to do the things I love.

Contents

Part I

Overview

CHAPTER 1

Introduction

1.1 Introduction

Colloquially, fluids are defined as substances that deform continuously under the application of an external force and solids are substances that resist deformation. Simply put, fluids flow and solids do not. By this definition, mayonnaise is a solid as it maintains its shape against gravity and window glass is a fluid as it creeps and deforms, albeit ever so slowly [1]. Although the classical definition seems to work fine for many materials, it is inadequate to describe many materials of everyday use and of engineering applications. This includes rubbery, gooey, slimy and pasty substances that are difficult to strictly classify as either solids or fluids. Such materials are commonly known as complex fluids as they show both solid and liquid like behaviour. Before going into the science of complex fluids and their flow, it is important to develop a framework that can be used to define different types of fluids and understand the mathematical models that govern them.

1.2 Governing Equations

Considering the fluid as a continuum, the Navier-Stokes equations that govern the flow of incompressible fluids can be derived starting from Cauchy's momentum equations [2]. Applying the momentum conservation equation ($\Sigma F = ma$) to an infinitesimal volume of fluid subject to body forces, the convective form of the Cauchy's equation is given by:

$$\rho \frac{D\boldsymbol{v}}{Dt} = \nabla \cdot \mathbf{T} + \rho \mathbf{f} \tag{1.1}$$

where,

- $\frac{D\boldsymbol{v}}{Dt} = \frac{\partial \boldsymbol{v}}{\partial t} + \boldsymbol{v} \cdot \nabla \boldsymbol{v}$ is the material derivative of the velocity vector $\boldsymbol{v} = \boldsymbol{v}[\boldsymbol{x}(t), t]$
- ρ is the density of the continuum
- $\boldsymbol{f} = \begin{bmatrix} f_x \\ f_y \\ f_z \end{bmatrix}$ is the body force acting on the continuum
- $\nabla = \left[\boldsymbol{e_x} \frac{\partial}{\partial x} + \boldsymbol{e_y} \frac{\partial}{\partial y} + \boldsymbol{e_z} \frac{\partial}{\partial z} \right]$ is the nabla operator and $\boldsymbol{e_x}, \boldsymbol{e_y}$ and $\boldsymbol{e_z}$ are unit vectors in x, y and z directions respectively
- $\mathbf{T}$ is the stress tensor (symmetric), given by:

$$\mathbf{T} = \begin{bmatrix} \sigma_{xx} & \sigma_{xy} & \sigma_{xz} \\ \sigma_{yx} & \sigma_{yy} & \sigma_{yz} \\ \sigma_{zx} & \sigma_{zy} & \sigma_{zz} \end{bmatrix}$$

A simple constitutive relation can be used to express the stress tensor as a summation of the isotropic and deviatoric stress components. The stress tensor can then be mathematically expressed as:

$$\mathbf{T} = -p\mathbf{I} + 2\eta\mathbf{D} \tag{1.2}$$

where,

- p is the isotropic pressure
- η is the dynamic shear viscosity, and
- the rate of strain tensor $\mathbf{D} = \frac{1}{2}(\nabla \boldsymbol{v} + \nabla \boldsymbol{v}^T)$

The continuity equation can be represented as:

$$\nabla \cdot \boldsymbol{v} = 0 \tag{1.3}$$

The divergence of the deviatoric stress component in Eq 1.2 can then be written as:

$$2\eta \nabla \cdot \mathbf{D} = \eta \nabla \cdot (\nabla \boldsymbol{v} + \nabla \boldsymbol{v}^T) = \eta \nabla^2 \boldsymbol{v}$$

Substituting the expression for the divergence of the stress tensor in Cauchy's momentum equation (Eq 1.1), we get the famous Navier-Stokes equation (incompressible fluid case)

$$\rho \cdot \left(\frac{\partial \boldsymbol{v}}{\partial t} + (\boldsymbol{v} \cdot \nabla)\boldsymbol{v} \right) = -\nabla p + \eta \nabla^2 \boldsymbol{v} + \rho \mathbf{f} \tag{1.4}$$

Expanding Eq 1.2 we get

$$\begin{bmatrix} \sigma_{xx} & \sigma_{xy} & \sigma_{xz} \\ \sigma_{yx} & \sigma_{yy} & \sigma_{yz} \\ \sigma_{zx} & \sigma_{zy} & \sigma_{zz} \end{bmatrix} = \begin{bmatrix} -p & 0 & 0 \\ 0 & -p & 0 \\ 0 & 0 & -p \end{bmatrix} + ...$$

$$2 \times \frac{1}{2}\eta \begin{bmatrix} 2\dfrac{\partial v_x}{\partial x} & \dfrac{\partial v_x}{\partial y} + \dfrac{\partial v_y}{\partial x} & \dfrac{\partial v_x}{\partial z} + \dfrac{\partial v_z}{\partial x} \\ \dfrac{\partial v_y}{\partial x} + \dfrac{\partial v_x}{\partial y} & 2\dfrac{\partial v_y}{\partial y} & \dfrac{\partial v_y}{\partial z} + \dfrac{\partial v_z}{\partial y} \\ \dfrac{\partial v_z}{\partial x} + \dfrac{\partial v_x}{\partial z} & \dfrac{\partial v_z}{\partial y} + \dfrac{\partial v_y}{\partial z} & 2\dfrac{\partial v_z}{\partial z} \end{bmatrix}$$

In simple shear flows $\sigma_{xz} = \sigma_{zx} = \sigma_{yz} = \sigma_{zy} = 0$, and considering a pure viscous fluid $\sigma_{xx} = \sigma_{yy} = \sigma_{zz} = 0$. Further considering the symmetry of the stress tensor

$$\sigma_{xy} = \sigma_{yx} = \eta \left(\frac{\partial v_x}{\partial y} + \frac{\partial v_y}{\partial x} \right) \tag{1.5}$$

In the case of a Newtonian fluid flowing between two parallel plates, one moving at a constant velocity v_x and the other stationary (Fig 1.1), $\frac{\partial v_x}{\partial y} = 0$, and the shear rate in simple shear flows can be defined as:

$$\dot{\gamma}_{xy} = \frac{\partial v_y}{\partial x} \tag{1.6}$$

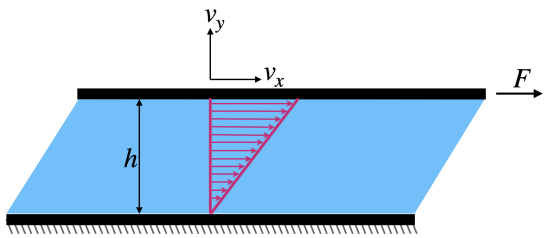

Figure 1.1: Simple shear flow

Eq 1.6 then becomes

$$\sigma_{xy} = \sigma_{yx} = \eta_0 \dot{\gamma}_{xy} \tag{1.7}$$

where, η_0 is the viscosity of a Newtonian fluid.

Eq 1.7 is called Newton's law of viscosity. Fluids including water, most gases, alcohols and molten metals are often termed as Newtonian fluids. For a Newtonian fluid, at constant temperature and pressure, the shear stress (σ) in simple shear flow is linearly dependent on the shear rate ($\dot{\gamma}$) through a constant of proportionality known as the shear viscosity (η) (see Eq 1.7). Since the development of the mass and momentum equations (Cauchy, Navier-Stokes) 300 years ago, the understanding of Newtonian flows has come a long way and their predictions through analytical and computational means have become easier and more robust, although challenges in turbulence and multiphase flows still remain. Early on in this timeline of understanding of Newtonian fluids, it was observed that a vast majority of commonly used fluids did not follow the linear $\sigma - \dot{\gamma}$ Newtonian regime. These fluids started to be known as non-Newtonian fluids. Non-Newtonian fluids exhibit a broad range of rheological properties that are not shown by Newtonian fluids, which makes their characterization and as a result their flow predictions challenging.

The terms ‘complex fluid’ and ’soft matter’ are often used interchangeably with non-Newtonian fluids and are used to describe materials having mesoscopic length scales and a hierarchical structure that give rise to complex rheological properties and flow properties [3]. Complex fluids also include multiphase systems such as solid-liquid (suspensions), solid-gas (granular), liquid-liquid (emulsions) and liquid-gas (foams). In general, complex fluids can be thought of fluids exhibiting ′complex′ behaviour in terms of material and flow properties [4]. This includes natural fluid systems such as molten lava, clay and avalanches; food products such as yogurt, honey and chocolate; household products such as toothpaste, paints and grease; bodily fluids such as blood and many industrial fluids and chemicals such as Carbopol and Laponite to name a few.

1.3 Rheological properties

Basic rheology of non-Newtonian fluids

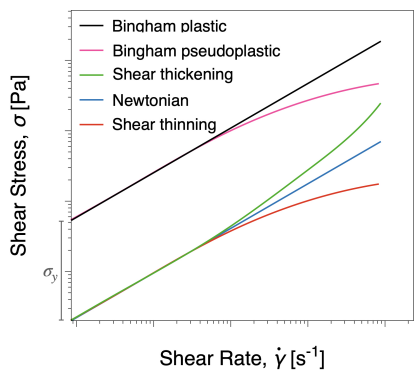

Figure 1.2: Representative flow curves of Newtonian, shear-thinning, shear-thickening, Bingham plastic and Bingham pseudoplastic fluids.

Non-Newtonian fluids show a nonlinearity in the $\sigma - \dot{\gamma}$ relationship. Based on the relations, some basic rheological behaviours can be identified. Shear-thinning (or pseudoplasticity) is a rheological property of many non-Newtonian

fluids where the shear viscosity of the fluid decreases with an increase in shear rate [5]. This is a characteristic behaviour of many materials where the internal structure suffers conformational changes upon the application of shear, aligning in the flow direction and resulting in lower resistance to flow or a decrease in viscosity as the shear rate is increased [6]. On the contrary, shear-thickening fluids (or dilatant fluids) register an increase in viscosity as the shear rate is increased. Although a rare phenomenon, shear-thickening is observed for fluids like cornstarch solution and water soaked sand. Bingham plastic and Bingham pseudoplastic fluids are characterized by a yield stress that needs to be overcome for the fluid to start flowing. Once the yield stress is overcome, the fluid may start flowing like a Newtonian fluid (Bingham plastic) or a shear thinning fluid (Bingham pseudoplastic). The rheology of yield stress fluids and their measurement methods are explained in detail in the upcoming sections of this thesis. The flow curves for the different types of fluids discussed are represented in Fig 1.2.

The shear-thinning and thickening behaviour of fluids can be modeled using the Ostwald-de Waele equation, famously known as the power law model [7]

$$\sigma = K\dot{\gamma}^n \tag{1.8}$$

where, K is the consistency index and n is the power law index or the flow mode.

$$n < 1 \rightarrow \text{Shear thinning}$$
$$n = 1 \rightarrow \text{Newtonian}$$
$$n > 1 \rightarrow \text{Shear thickening}$$

Whereas, the Bingham plastic and Bingham pseudoplastic fluids can be modeled using viscoplastic relations shown in Eq 1.9 and Eq 1.10 respectively.

$$\sigma = \sigma_y + K\dot{\gamma} \tag{1.9}$$

$$\sigma = \sigma_y + K\dot{\gamma}^{n<1} \tag{1.10}$$

where σ_y is the yield stress of the fluid.

Note that more advanced constitutive equations exist that model the shear thinning behaviour of fluids such as the Cross model [8] and Carreau model [9].

Linear viscoelasticity

Viscoelasticity is a property of materials that exhibit both solid and liquid like characteristics while undergoing deformation. The elastic component refers to the ability of a material to undergo reversible elastic deformation while the viscous component refers to its dissipation ability through flow [6]. One of the common methods to measure linear viscoelasticity is by performing dynamic oscillatory tests using a rheometer. The stored deformation energy is given by the storage modulus (G'), while the deformation energy dissipated by the material through internal friction is represented by the loss modulus (G''). Typically, to measure the viscoelastic behaviour of a material, first a strain sweep is performed at a constant angular frequency.

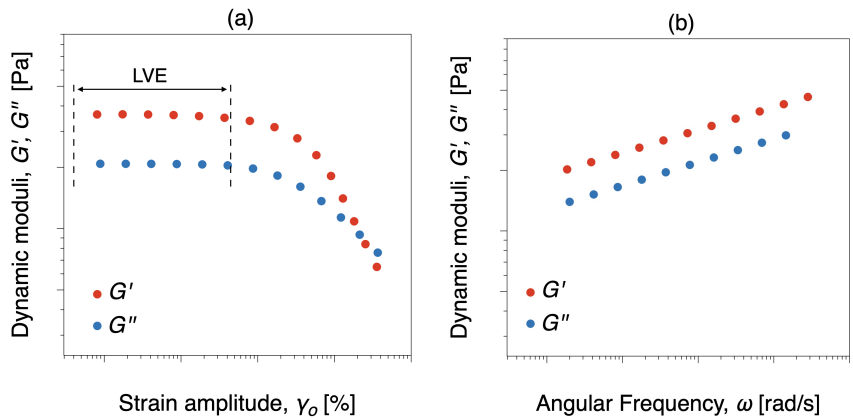

Figure 1.3: Representative dynamic (a) shear strain sweep and (b) angular frequency sweep test results.

The linear viscoelastic (LVE) region can be thus identified as extending up to the strain amplitude limit where the dynamic moduli are independent of the strain amplitude. Thereafter, angular frequency sweep tests can be performed at a constant LVE shear strain amplitude [10]. The frequency sweep test describes the time dependent response of the material structure in the non-destructive deformation range (LVE region). Representative shear strain sweep and angular frequency sweep test results for a fluid with elastic dominated material response ($G' > G''$) are presented in Fig 1.3. Note that these figures are just representations of what an ideal oscillatory test result could

look like. In reality, the dynamic moduli response can be very different based on the material under consideration and interesting insights can be obtained from these tests. For example, materials which show an elastic-dominated response,$G' > G''$, over the entire frequency spectrum are usually called gels (gel-like behavior); whereas if $G' < G''$ then material has a dominant viscous response or fluid-like behaviour. A measure of the gel strength of a material can be given by the loss factor by Eq 1.11.

$$\tan\delta = \frac{G''}{G'} \tag{1.11}$$

Viscoplasticity or Yield Stress

Many complex fluids exhibit a viscoplastic behaviour when deformed. Viscoplasticity is the characteristic of many materials to undergo plastic deformation when a stress greater than the yield stress is applied on to the material [6]. Beyond the yield stress the material starts to flow. Many different methods have been proposed in the literature to measure the yield stress, some of which are described below. These tests have different inputs and produce different yield stress results based on the protocol followed.

Two distinct yield stresses exist for any given fluid. The stress required to be overcome to initiate plastic deformation is called the static yield stress. Whereas, the stress required to maintain plastic deformation or flow is known as dynamic yield stress. It can be considered as the stress required to cease the flow.

Shear rate controlled steady shear test

A widely used method to determine the yield stress of a material is by performing shear rate controlled steady shear test and fitting a viscoplastic constitutive equation to the flow curve of the material. A common model used for this purpose is the Herschel-Bulkley equation [11]:

$$\sigma = \sigma_y + K\dot{\gamma}^n \tag{1.12}$$

where, σ_y is the yield stress and, K and n are the consistency index and the flow index respectively. The Herschel-Bulkley model is fitted to the flow curve of the material and extrapolated to $\dot{\gamma} = 0$. The distance from the origin where

the fitted curve intersects the ordinate is taken as the static yield stress if the flow curve is obtained by performing ramp up in shear rate, and dynamic yield stress if the flow curve is obtained through ramp down in shear rate [11]. Note that unlike a pure shear thinning material, the flow curve of a material exhibiting yield stress doesn't pass through the origin, suggesting that an initial stress has to be overcome for the material to start flowing. A typical Herschel-Bulkley fit to determine the yield stress is represented in Fig 1.4(a).

Stress controlled steady shear test

Another widely used method of measuring the static yield stress is by performing stress controlled steady shear stress tests where the shear viscosity function is measured as the shear stress is ramped up. A decrease in viscosity can be observed as the material undergoes plastic deformation. Shear stress corresponding to the intersection point between the tangents drawn on the viscosity function is considered as the yield stress of the material [12]. A typical steady shear stress test curve is represented in Fig 1.4(b).

Creep test

It can be observed from the steady shear stress curve in Fig 1.4(b) that the decrease in the shear viscosity function is not sudden. For most materials, the viscosity function decreases gradually, suggesting that the material yields over a wide range of shear stresses. This range in which the material undergoes plastic deformation can be measured in a creep test [13]. In such tests, the transient shear viscosity response is measured at constant input shear stresses. When a shear stress greater than the yield stress of the material is applied, the viscosity function decreases with time due to structural breakdown. However, when a shear stress less than the yield stress range of the material is applied, the structure of the material builds up resulting in an increase in viscosity. In the yield stress range the viscosity response fluctuates as the material goes towards its steady state, starting from a transient state. The range of input shear stresses which result in the fluctuation of the viscosity function is considered as the static yield stress range. Furthermore, this test protocol is also used to observe the transient material response and measure the time required to achieve steady state. A representative graph of such a test is presented in

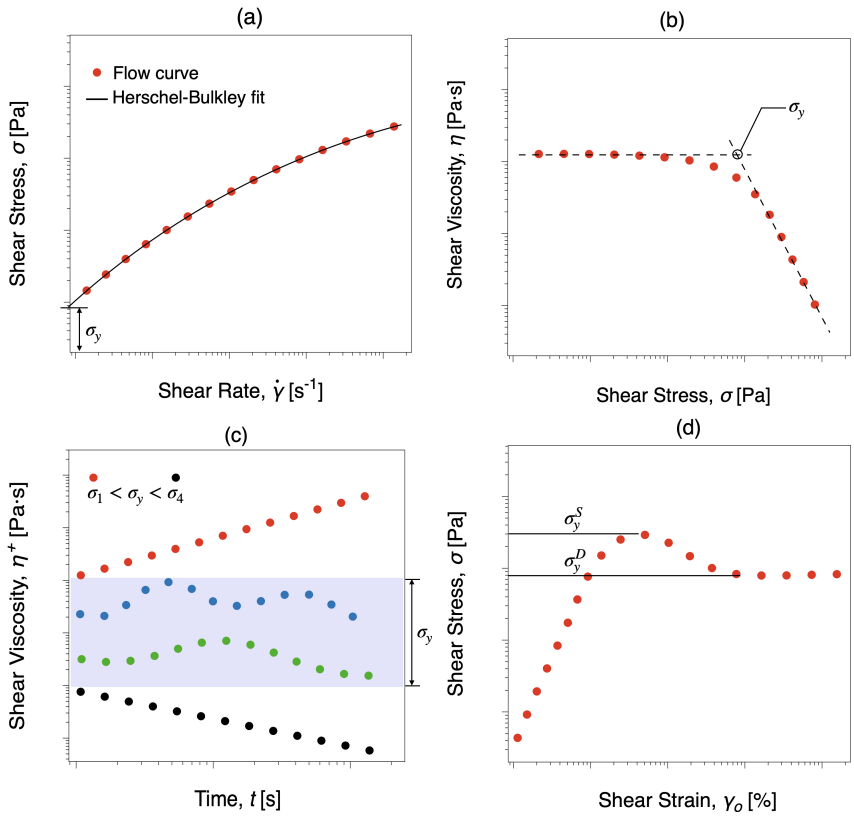

Figure 1.4: Rheological tests to measure yield stress: (a) shear rate controlled steady shear test, (b) stress controlled steady shear test, (c) creep test and (d) start-up test.

Fig 1.4(c).

Start-up test

In a start-up flow test, the shear strain is ramped up at a constant rate as the shear stress response of the material is recorded [14]. The material first deforms elastically. This is a reversible deformation and the material goes back to its original state if the strain is reduced to 0 in this range. However, beyond a critical strain, the material yields and starts flowing. This is the static yield stress of the material. The shear stress then decreases and attains a plateau. Stress corresponding to the plateau region is the dynamic yield stress of the material. A representative shear stress-shear strain curve is shown in Fig 1.4(d).

Note that other methods of determining the yield stress have also been proposed in the literature, such as in oscillatory tests [11]. The dynamic yield stress can be measured from oscillatory tests by performing a shear stress ramp and measuring the dynamic moduli. Tangents are then drawn on the storage modulus curve (usually) and the shear stress corresponding to the intersection between the tangents is taken as a measure of the yield stress. However, sometimes the crossover point between G' and G'' is also considered as the yield stress [11].

It is evident that different tests result in different measure of yield stress and based on the measuring protocol one could be measuring either the static or the dynamic yield stress. Additionally, for fluids showing time dependent material rheology, the measurement of yield stress becomes especially challenging as the yielding phenomenon is affected by the time period of shearing. These factors add to the complexity of measuring yield stress fluids.

Thixotropy

Thixotropy is a characteristic behaviour of many yield stress materials wherein the structure of the material breaks down upon the application of shear and builds up with time when the shear is removed, beyond the time frame of the experiment [15]. Numerous measurement methodologies exist in the scientific literature to probe the thixotropic material behaviour, however, different test configurations yield contrasting results. As the thixotropic response of a material is time and shear rate dependent, attention must be paid to the

measurement protocol employed. Some of the typical thixotropic tests are highlighted below.

Hysteresis loop test

Hysteresis loop test is one of the most common methodologies used to measure thixotropy. It involves ramping up the shear rate step wise and measuring the flow curve of the material, followed by subsequent ramp down of shear rate [16]. As the shear rate is ramped up in shear rate controlled steady shear tests, the structure of the material breaks down and it recovers with time as the shear rate is ramped down. Due to the material undergoing structural breakdown with time, the flow curve obtained during the ramp down in shear rate is different and lower in magnitude than the flow curve obtained in ramp up. This gives rise to a hysteresis loop, the area of which is often considered a measure of thixotropy [16]. In hysteresis loop tests shear rate and time are coupled. The magnitude of stress response varies with the choice of time step size at each discrete shear rate. If a time step size equal to the material's steady state time is allowed at each shear rate, the structure of the material breaks down significantly (sometimes beyond repair), affecting the shear stress response in subsequent shear rate steps. Therefore, typically the hysteresis loop tests are performed at the material's transient state. A representative hsyteresis loop is presented in Fig 1.5(a).

Multi Interval Thixotropic Test (MITT)

MITT is often performed to study the response of thixotropic materials to sudden changes in input shear rate [17]. It is also used to measure the effect of transient shear history on material behaviour and study its effects on material recovery time. Many different forms of MITT have been proposed in the scientific literature. The most commonly used method involves random step wise increase and decrease of shear rate levels and measuring the resulting shear stress or viscosity response. When a shear rate corresponding to shear stress lower than the yield stress of the material is applied, an increase in shear viscosity response can be observed due to structural buildup, and when a shear rate corresponding to shear stress higher than the yield stress is applied, the shear viscosity decreases with time due to structural breakdown. The shear rate input may not be random for some MITT measurements and may involve

a gradual decrease followed by a gradual increase in shear rate levels or vice versa. A special form of MITT test, called the three interval thixotropic test (3ITT) consists of only three intervals of input shear rates, usually having a high input shear rate in the second interval with the first and third intervals being identical [16]. 3ITT is used to study the material's recovery response without a shear history in the first interval, followed by destroying the material structure in the second interval by employing a high shear rate and finally measuring the change in material's recovery response in the third interval where the shear rate level is same as the first interval. Similar to hysteresis loop tests, the material response is significantly affected by the choice of time step size chosen for each interval. A typical MITT test is shown in Fig 1.5(b).

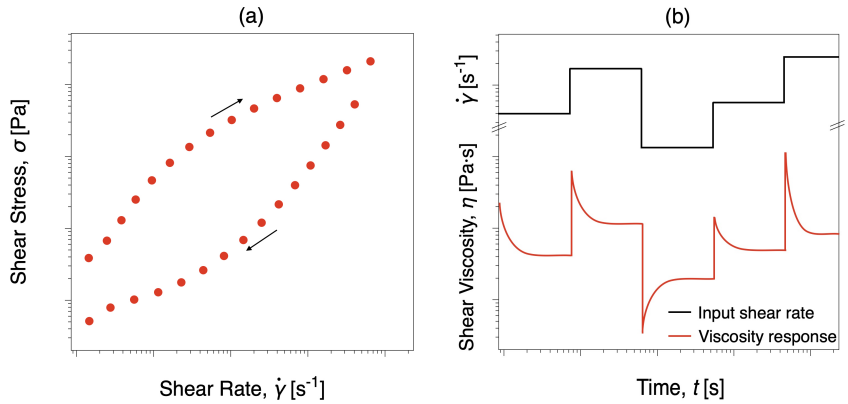

Figure 1.5: Rheological methods to measure thixotropy: (a) hysteresis loop test and (b) multi interval thixotropic test (MITT).

The three step oscillation test is a variation of the 3ITT test which involves recording the dynamic moduli response to three input shear rate levels [18]. Start-up tests are another variation where the material is pre-sheared and then allowed to rest. A sudden application of shear rate after the rest period results in a stress overshoot followed by the stress reaching a plateau towards the steady state of the material [19]. The effect of material's thixotropy is studied as a function of the stress overshoot and rest time allowed after pre-shear.

It is evident that many different methods of measuring yield stress and thixotropy exist in the scientific literature. Materials exhibiting only yield

stress are known as simple yield stress fluids, because materials that exhibit both yield stress and thixotropy are more complex and challenging to characterize. For a thixotropic material, the yield stress also becomes a function of time and the structural breakdown due to yielding competes with structural recovery with time due to thixotropy. Therefore, it has been claimed that yield stress and thixotropy manifest from the same basic physics [20] and it is extremely challenging to decouple them. Additionally, some complex fluids are known to exhibit time dependent viscoelasticity and, similar to thixotropic materials, form a hysteresis loop in shear rate controlled steady shear tests. It is especially challenging to decouple thixotropic and viscoelastic effects, although recent studies have tried to understand the differences between the two [21]. Moreover, microstructural changes that affect viscoelasticity and give rise to overshoot in dynamic moduli in oscillatory tests, also affect the viscoelastic response of the material and its yield stress [22]. The coupling between the various complex rheological material behaviour adds to the complexity of the fluid and its measurement.

1.4 Motivation and present work

Complex fluids have wide spread applications in industries and products of daily use. However, they exhibit complex rheological material behaviour which makes their characterization challenging [23]. To enhance their production and processing efficiency, these rheological properties need to be properly characterized and the flow properties of these fluids studied and predicted. Numerous attempts have been made to study the sometimes elusive material properties of these complex fluids and many constitutive models have been proposed to predict their flow behaviour [15], [20], [24]–[29]. However, due to inadequate measurement protocols and constitutive modeling of the transient material behaviour, we still lack proper understanding and predictability of most of these complex fluids [30]. The goal of this PhD project is to predict the flow behaviour of complex fluids in different test configurations such as milifluidic channels, pipes and surfaces through implementing adequate constitutive models, supported by improved rheological and microstructural characterizations.

In this particular thesis we have taken preliminary steps towards studying the rheological properties and microstructure of three widely used complex

fluids, predicted their rheology using constitutive modeling and performed experimental flow visualization in milifluidic channels. We started with introducing the topic and discussing the various existing methods of characterization of the rheological properties of interest such as viscoelasticity, yield stress and thixotropy in chapter 1. In chapter 2 the materials studied in this thesis are presented and the methods used for rheological characterization, numerical modeling, microstructural imaging and flow visualization in milifluidic channel are discussed. In chapter 3, some of the key results are highlighted and finally in chapter 4 concluding remarks and future scope are presented.

CHAPTER 2

Materials and Methods

The goal of this PhD programme is to study the flow dynamics of complex fluids. For this particular study, we have chosen three different fluids showing complex rheology and flow properties. These are:

(a) Yogurt: a food product widely used all over the world, it is a live sample formed through fermentation by bacterial culture. The microstructure of yogurt consists of protein and casein network, along with fat globules and/or additives. The material properties of yogurt highly depend on factors such as environmental and processing conditions, source of milk and additives used. Yogurt has been found to be a yield stress fluid showing thixotropic and viscoelastic material behaviour [31], [32]. We investigate the rheological and flow properties of three different types of yogurt in this study: Naturell, Vanilj and Långfil. They differ in their composition based on bacterial culture and flavour additives used. More information about the composition is provided in paper I.

(b) Carbopol: Carbopol is a synthetic polymer widely used in industries as a viscosity modifier, stabilizer, binder and adhesive. Different varieties of Carbopol are now available in the market. Carbopol solution is considered as a model fluid and has been widely studied because of its elasto-viscoplastic

properties [33]. Carbopol forms a hydrogel and does not exhibit thixotropic material behaviour under normal circumstances. However, it has been recently discovered that Carbopol solutions can be made to show thixotropic effects by modifying the sample preparation method [34].

(c) Laponite: Laponite is a synthetic polymer widely used to modify or enhance the rheology of many widely used fluids such as paints, inks, cosmetics and shampoos. When prepared in a solution form, it shows high thixotropy and elasto-viscoplastic behaviour [35].

Three different concentrations of Carbopol and Laponite were prepared for this study based on varying levels of rheological properties such as viscoelasticity, yield stress and thixotropy. The sample preparation and handling methods have been elaborated in paper II of this thesis.

2.1 Rheological characterization

Rheological properties of the three types/concentrations of yogurt, Carbopol and Laponite were characterized using an Anton Paar 702e Space rheometer in single motor transducer configuration. The C-ETD 200/XL cell accessory was used to maintain the temperature constant at 23 °C during all measurements. A custom built profiled bob and cup geometry with vertical profiling, CC27/P6, having an inner cup diameter of 29 mm and a bob diameter of 27 mm was used to minimize the effects of wall slip. Considering the transient and memory effects of the samples chosen, a fresh sample was used for every measurement to reduce the effect of shear history on measurement results.

The viscoelastic behaviour of the samples was measured through dynamic oscillatory tests. Shear strain amplitude sweep tests were performed at a constant angular frequency of 6 rad/s. Based on the linear viscoelastic range identified, angular frequency sweep tests were then performed at a constant shear strain amplitude of 0.1 %.

Yield stress of the three samples was estimated by performing stress controlled steady shear stress tests and measuring the viscosity function of the material. Additionally for yogurt samples, the yield stress range was measured through creep tests. The yield stress measured in steady shear stress test was used as a reference to choose the shear stress inputs of the creep test.

Thixotropic material behaviour was measured primarily through hysteresis loop tests. The shear rate was ramped up in the range of $\dot{\gamma} \in [10^0, 10^3]$

s^{-1} for yogurt and Laponite samples with a time step size of 120 s and 30 s respectively at each shear rate and then subsequently ramped down while measuring the shear stress of the samples. For Carbopol, a shear rate ramp up and down was performed in the range of $\dot{\gamma} \in [10^{-2}, 10^{2}]$ s^{-1}, with a time step size of 30 s. Additionally for yogurt samples, MITT tests were performed at 8 distinct shear rate intervals, with three of the intervals corresponding to shear stress below the yield stress of the samples and rest of the intervals having stress levels higher than the yield stress.

2.2 Numerical modeling

In paper I, numerical modeling has been used to fit four different phenomenological thixotropic models to hysteresis loop tests of yogurt samples and based on the values of the fitting parameters obtained, predict yogurt's thixotropic response in MITT tests. The thixotropic models considered consist of an equation of state (E.O.S), which represents the shear stress as a function of the shear rate and the so called structural parameter $\lambda(t)$. The E.O.S. for Mujumdar et al., (2002), Worrall & Tuliani, (1964) and Coussot et al., (2002) models is shown in equation 2.1.

$$\sigma[\lambda(t), \dot{\gamma}] = [K_1 + K_2\lambda(t)]\dot{\gamma}^m \tag{2.1}$$

The E.O.S of the fourth model by Schmitt et al., (1998) is given by

$$\sigma[\lambda(t), \dot{\gamma}] = \lambda(t)\sigma_i(\dot{\gamma}) = \lambda(t)k_i\dot{\gamma}^{n_i} \tag{2.2}$$

The structural parameter $\lambda(t)$ is a dimensionless quantity that represents the amount of structure present in the material, $\lambda(t) \in$ [0,1]. $\lambda(t) = 1$ represents fully structured network and $\lambda(t) = 0$ represents complete structural breakdown. $\lambda(t)$ is given by a kinetic or rate equation, where it is a function of shear rate, time and the structure at the previous time step. The kinetic equation of the thixotropic models chosen can be analytically solved to get an expression of $\lambda(t)$, which when simultaneously solved with the E.O.S, gives the shear stress response of the material. The four thixotropic models chosen are presented in Table 2.1.

Mujumdar et al., (2002), Worrall & Tuliani, (1964) and Coussot et al., (2002) models have a kinetic equation of the form

$$\frac{d\lambda(t)}{dt} = \underbrace{k_1\dot{\gamma}^a\lambda(t)^b}_{\text{Breakdown}} + \underbrace{k_2\dot{\gamma}^c[1-\lambda(t)]^d}_{\text{Buildup}}. \tag{2.3}$$

where the rate of change of the structural parameter depends on a breakdown and a buildup term. Based on the values of the indices a, b, c and d, the kinetic equations of the three models can be obtained.

The kinetic equation of the Schimitt et al., (1998) model is given by

$$\frac{d\lambda(t)}{dt} = -C[\lambda(t,\dot{\gamma}) - \lambda_e]^p \tag{2.4}$$

where $k_1, k_2, K_1, K_2, K_i, m, n_i, p$ and λ_e are model constants that are determined by fitting the E.O.S and the kinetic equation simultaneously to the hysteresis loop data obtained from measurements. The least squared error fitting methodology is explained in detail in paper I.

Table 2.1: Summary of thixotropic models consisting of an equation of state and kinetic equation used in the study.

Equation of State (EOS)	Author & Indices	Kinetic Equation
	Mujumdar et al., (2002) [29] $a=1,\ b=1,\ c=0,\ d=1$	$\frac{d\lambda(t)}{dt} = -k_1\dot{\gamma}\lambda(t) + k_2[1-\lambda(t)]$
$\sigma = [K_1 + K_2\lambda(t)]\dot{\gamma}^m$	Worrall & Tuliani, (1964) [36] $a=1,\ b=1,\ c=1,\ d=0$	$\frac{d\lambda(t)}{dt} = -k_1\dot{\gamma}\lambda(t) + k_2\dot{\gamma}$
	Coussot et al., (2002) [13] $a=1,\ b=1,\ c=0,\ d=0$	$\frac{d\lambda(t)}{dt} = -k_1\dot{\gamma}\lambda(t) + k_2$
$\sigma[\lambda(t),\dot{\gamma})] = \lambda(t)\sigma_i(\dot{\gamma})$ $= \lambda(t)K_i\dot{\gamma}^{n_i}$	Schmitt et al., (1998) [37]	$\frac{d\lambda(t)}{dt} = -C[\lambda(t,\dot{\gamma}) - \lambda_e]^p$

2.3 Flow visualization in milifluidic channel

A milifluidic flow setup was designed to study the influence of the rheological material behaviour on the flow field of the thixo-elasto-viscoplastic fluids. The rectangular milifluidic channel (cross section 1×3.25 mm^2) was created

by stacking 2 plexiglass plates and 2 aluminium plates on to a stainless steel plate. The milifluidic channel formed has a length of 80 mm. The flow visualization was performed using a Doppler-Optical Coherence Tomography (D-OCT) device at a distance of 65 mm from the starting point to minimize entrance effects. The D-OCT equipment works on the principles of Michelson interferometry to measure the difference in contrast in the flow and reconstructs the velocity field from the backscattered light using the principles of Doppler frequency shift [38], [39]. It has the ability to visualize the flow within the milifluidic channel by penetrating the flow field up to a depth of 2.58 μm. This enables non intrusive flow field visualization near the channel surface, giving interesting insights about the fluids' flow behaviour close to the wall surface. A schematic of the milifluidic channel setup is presented in Fig 2.1.

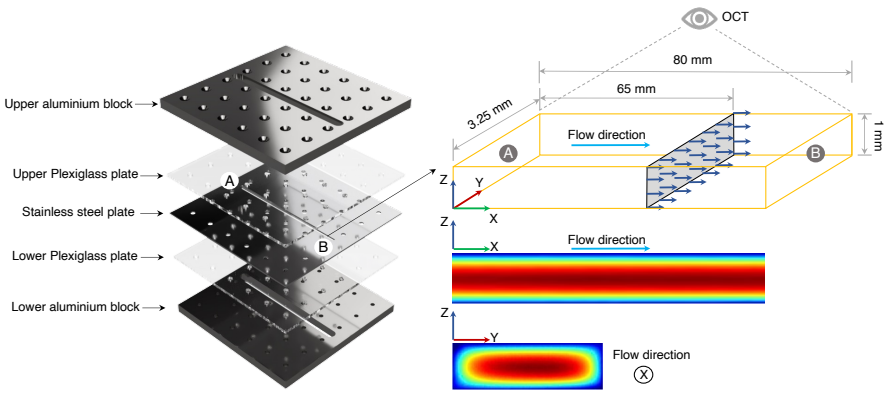

Figure 2.1: Schematic of the milifluidic channel setup.

500 consecutive frames of the velocity field were captured, which were then probed at specific locations to obtain the velocity profile. The fluid was pumped into the channel using a motorized syringe pump at three different flow rates of 0.4, 2.6 and 5 ml/min. The time taken by the fluid to reach the test section was noted, which varied significantly based on the material's yield stress, thixotropy and viscoelastic properties.

Ex-situ rheological measurements were performed to estimate the stress distribution inside the milifluidic channel. Shear rate profile was first calculated from the velocity profile data, which was then probed at 4 discrete depths

inside the channel. At these 4 selected shear rates, creep tests were performed and the shear stress evolution with time was measured. The test was stopped at the time equal to the time taken for the fluid to reach the test section and the shear stress at this point was noted. Finally, the shear stress data collected at different depths and flow rates was compiled to obtain the stress maps of the fluids. More details about the milifluidic channel and the workings of the OCT can be found in paper II of this thesis.

2.4 Microstructural characterization

Microstructural characterization was performed to understand the length scales of the fluids' structure that are representative of their complex behaviour. Scanning electron microscopy (SEM) was performed on the yogurt samples (see paper I). To investigate the effects of thixotropy on the material structure, yogurt samples were extracted at different stages during hysteresis loop test. The first sample was at rest, the second sample was extracted at shear rate of 1000 s^{-1} and the third sample was extracted at the end of the hysteresis loop test. This was done to observe the changes in the microstructure when it had broken down significantly at the highest shear rate and its ability to recover when the shear was removed. After extraction of the samples from the cup geometry, the structure was immediately arrested using liquid nitrogen. Thereafter, the samples were freeze dried to eliminate the water content from the structure. After 72 hrs of freeze drying, the samples were sputtered with gold to increase conductivity and visualized using SEM. Furthermore image processing was done to quantify the amount of structural breakdown and recovery of the samples (paper I).

CHAPTER 3

Results and discussions

Some key results obtained in this study are presented in this section. First the rheological material behaviour of yogurt, Carbopol and Laponite samples are presented in viscoelastic, yield stress and thixotropic tests (paper I and II). Then the numerical modeling results of the thixotropic models considered for one of the yogurt samples is briefly highlighted and the microstructural changes in yogurt due to its thixotropy are presented (paper I). Finally, the results of the flow visualization in a milifluidic channel are presented for the yogurt samples (paper II).

3.1 Linear viscoelasticity

The viscoelastic behaviour of the 3 yogurt samples (Naturell (Y^N), Vanilj (Y^V) and Långfil (Y^L)), 3 Carbopol samples having concentrations of 0.1 % ($C^{0.1\%}$), 0.2 % ($C^{0.2\%}$) and 0.6 % ($C^{0.6\%}$), and 3 Laponite samples with concentrations 1 % ($L^{1\%}$), 2 % ($L^{2\%}$) and 3 % ($L^{3\%}$) were compared by performing oscillatory strain sweep and angular frequency sweep tests in Fig 3.1. All the samples considered show a gel behaviour ($G' > G''$) in the linear viscoelastic range, with Carbopol ($\tan\,\delta \sim 0.06$) and Laponite ($\tan\,\delta \sim 0.03$) samples

forming stronger gels than yogurt (tan $\delta \sim 0.2$). It can also be observed that the elastic material response increases with concentration for Carbopol and Laponite, while for yogurt, Y^L shows lower elasticity as compared to Y^N and Y^V. Carbopol and Laponite samples also exhibit weak strain overshoot, given by the rise in G'' at the end of the linear viscoelastic region.

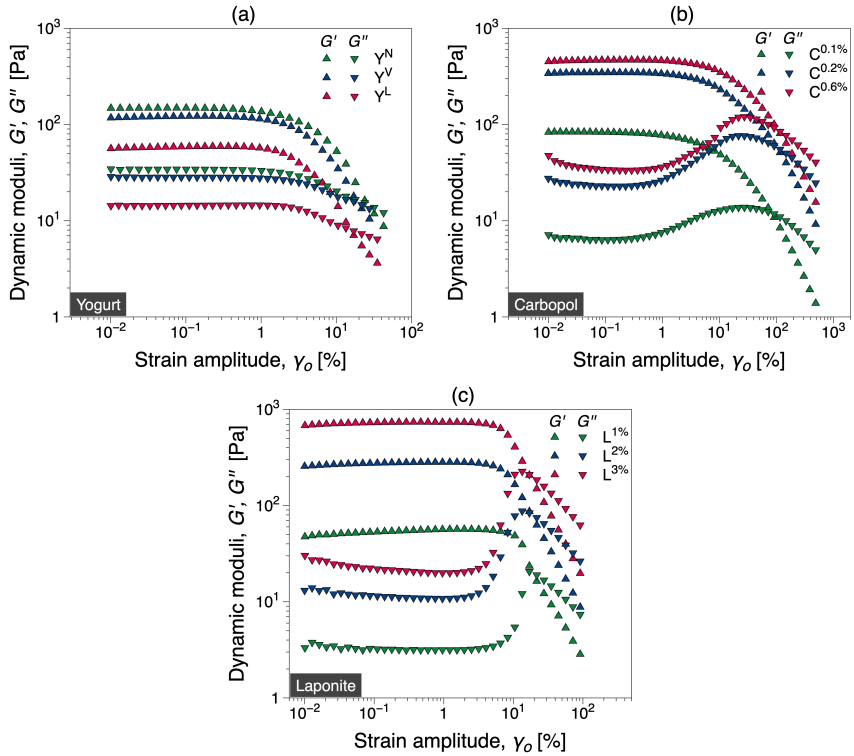

Figure 3.1: Oscillatory shear strain sweep test results for (a) yogurt, (b) Carbopol and (c) Laponite samples.

3.2 Yield stress

Some of the steady shear stress test results to measure the yield stress are presented in Fig 3.2. The three yogurt samples considered do not show a

significant difference in their yield stress values, however, for Carbopol and Laponite, the yield stress increases significantly with concentration.

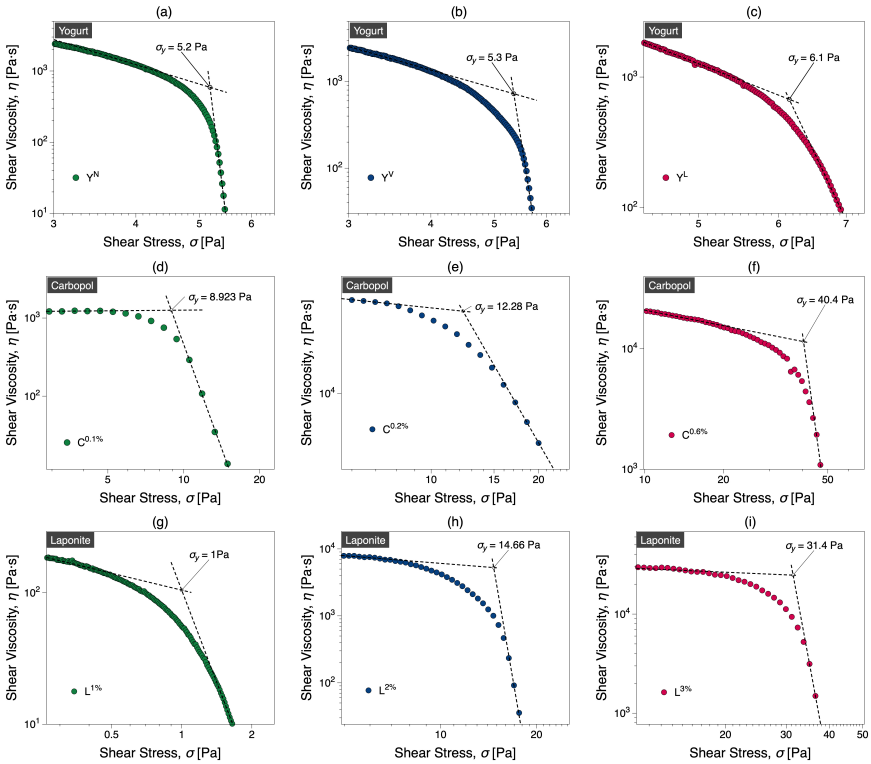

Figure 3.2: Steady shear stress tests for measurement of yield stress for (a)-(c) yogurt, (d)-(f) Carbopol and (g)-(i) Laponite samples.

3.3 Thixotropy

Thixotropic material behaviour was measured by performing hysteresis loop tests. All three yogurt samples show thixotropic response, with Y^L having the highest thixotropy among all 3 yogurts, based on the area of the hysteresis loop. For Carbopol and Laponite, the lowest concentrations ($C^{0.1\%}$ and $L^{1\%}$) are not thixotropic i.e., the flow curves during ramp up and down in

shear rate superimpose. However the thixotropy increases with concentration, with $C^{0.6\%}$ and $L^{3\%}$ being highly thixotropic. Hysteresis loop curves for all 9 samples are presented in Fig 3.3.

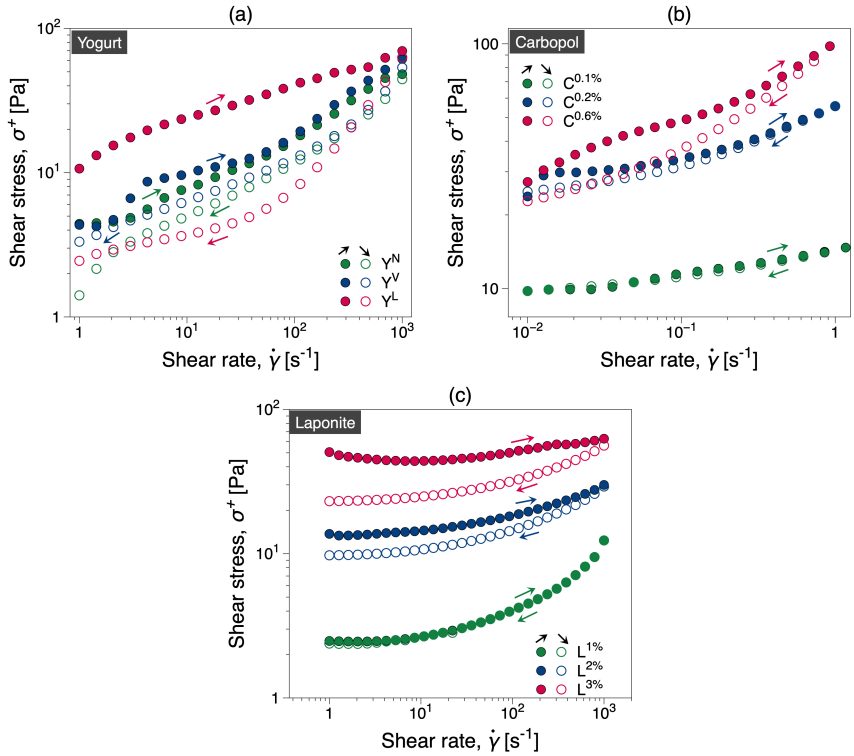

Figure 3.3: Thixotropic material response of (a) yogurt, (b) Carbopol and (c) Laponite in hysteresis loop test.

3.4 Numerical modeling

Numerical modeling was performed to predict the thixotropic material behaviour of the yogurt samples. The thixotropic constitutive models were used to fit the hysteresis loop test data. Based on the values of the model constants obtained, the complete models were used to predict the shear stress response

in MITT tests. More details about the fitting results and predictions can be found in paper I. However, the hysteresis loop fit, the corresponding shear stress and shear viscosity fit and the MITT predictions for Y^N are presented in Fig 3.4 and Fig 3.5 respectively.

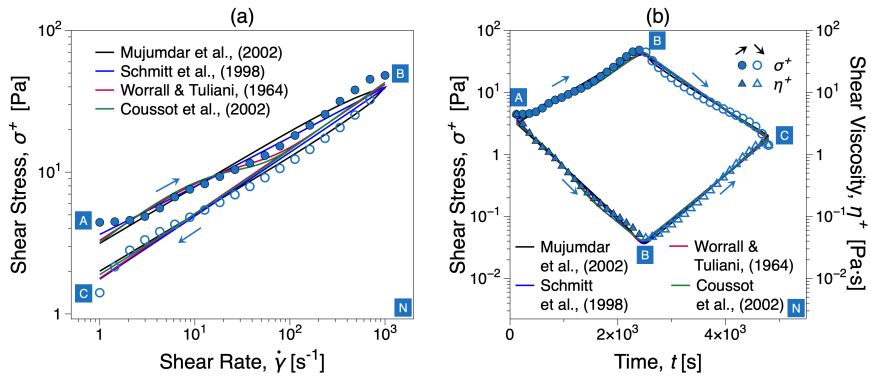

Figure 3.4: Figures showing fitting of the thixotropic models to the (a) hysteresis loop test of Y^N and the corresponding (b) shear stress and shear viscosity response with time.

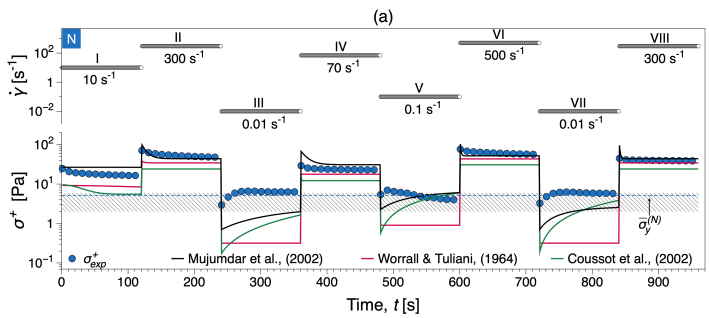

Figure 3.5: Numerical modeling predictions of the shear stress response in MITT test for yogurt sample Y^N.

While some models fit better in hysteresis loop tests, others predict the MITT tests better. A detailed error analysis of the fits and predictions are presented in paper I along with a discussion about the predictive power of the

thixotropic models considered.

3.5 Microstructural imaging

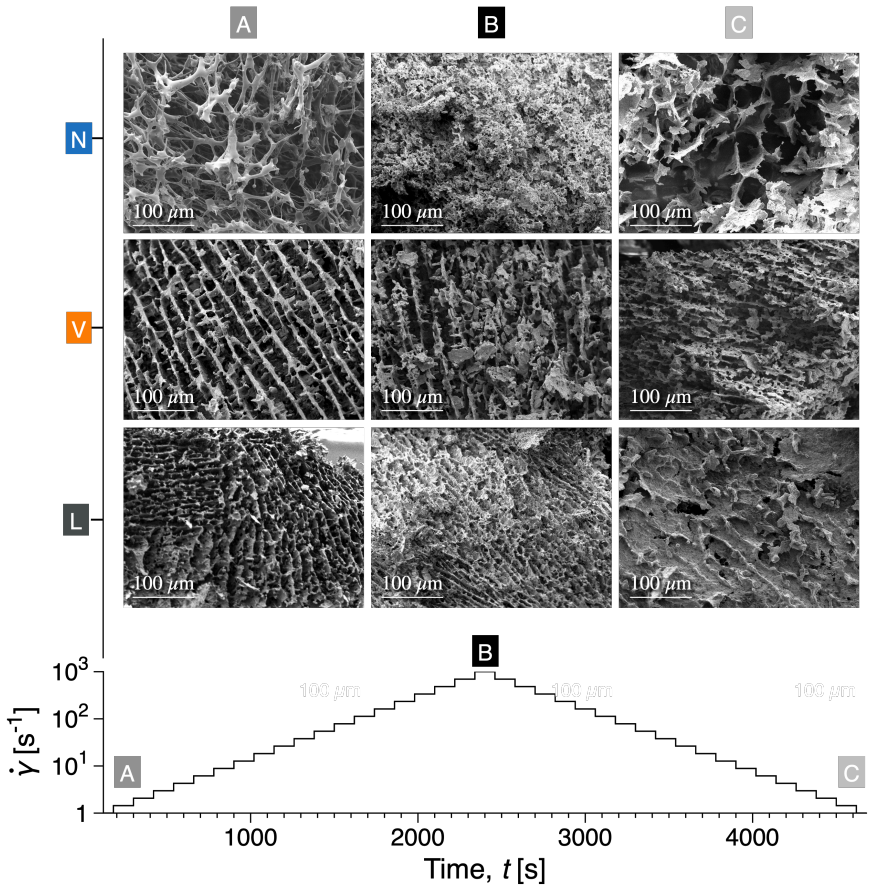

Figure 3.6: SEM micrographs of yogurt samples at three different shear rate levels in a hysteresis loop test.

SEM micrographs for the three yogurt samples are presented in Fig 3.6 at three different shear rate levels in the hysteresis loop test. Level A represents

unsheared sample, level B captures the yogurt microstructure at the highest shear rate of 1000 s^{-1} and level C represents the microstructure at the end of the hysteresis loop test. It can be observed that a considerable change occurs when the shear rate is varied. As the shear rate is increased, the structure breaks down and some recovery can be observed when the shear rate is reduced. However, for Y^L, the structure progressively breaks down even at the end of the hysteresis loop test because of the structural breakdown dominating over time due to the sample's high thixotropy. Quantitative analysis performed through image processing shows the level of interconnectivity between the branches changing with shear rate (see paper I).

3.6 Flow in milifluidic channel

The flow field of the samples in a milifluidic channel was visualized using D-OCT. To study the influence of thixotropy on the velocity field, in addition to the 9 samples considered, all the samples were stirred using an overhead mixer to break the structure before pumping it into the milifluidic channel. While the unstirred sample is termed as 'US', the stirred samples are named as 'S' for the purpose of comparison. The velocity field obtained was probed near the wall surface and the resulting velocity profiles for yogurt samples at three different flow rates are shown in Fig 3.7.

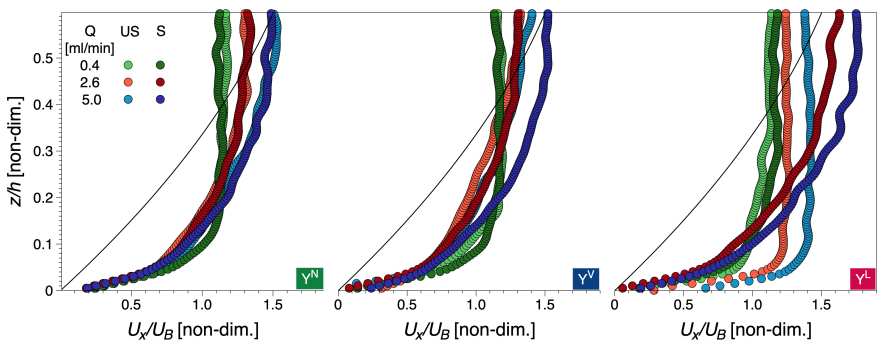

Figure 3.7: Figure showing the velocity profiles of unstirred and stirred yogurt samples at three different flow rates.

For all cases, a clear plugged profile can be observed, deviating from the ana-

lytical solution of the Newtonian velocity profile given by Boussinesq equation (black line). For Y^N the velocity profiles of the stirred and unstirred samples practically overlap on each other, showing that once plastic deformation has occurred, the additional structural breakdown caused by stirring the samples does not have a profound effect on the velocity profile near the surface as the structure quickly recovers due to lower thixotropy of the sample. For Y^V the velocity profile at the lowest flow rate shows higher plugged behaviour as the low flow rate gives the sample enough time to recover from the structural breakdown caused due to flow. For Y^L samples, more profiles can be observed to be engaged in the plug regime. The velocity profiles at all flow rates of the unstirred sample and the velocity profile at the lowest flow rate of the stirred sample show a profound plugged profile due to the structural recovery dominating the structural breakdown. The shear stress measured through creep tests at 4 discrete shear rate levels along the depth of the channel for both stirred and unstirred samples at 3 different flowrates were consolidated to construct the shear stress distribution map shown in Fig 3.8(a) and (b) for the unstirred and stirred cases respectively. The corresponding Reynolds (Re) and Bingham (Bi) numbers calculated from Eq 3.1 and Eq 3.2 respectively are also highlighted.

$$Re = \frac{\rho\, U_{bulk}\, h}{\eta} \tag{3.1}$$

$$Bi = \frac{\sigma_y\, U_{bulk}}{\eta\, h} \tag{3.2}$$

Where, ρ is the fluid density, U_{bulk} is the bulk velocity of the flow, h is the depth measured by distance from the channel wall, σ_y is the yield stress and η is the shear viscosity of the sample. Re and Bi are important dimensionless quantities that provide insights into the flow behaviour of the fluid. While Re is the ratio of inertial forces to viscous forces, Bi is the ratio of yield stress to viscous forces. By following the evolution of these 2 quantities along the channel depth, the interplay between inertial forces, viscous forces and yield stress can be studied.

The shear stresses recorded for the unstirred samples are higher than the stirred samples, because the structure of the material breaks down significantly upon stirring. The imposed stress propagates easily through the material structure. However, for more structured material, the microstructure

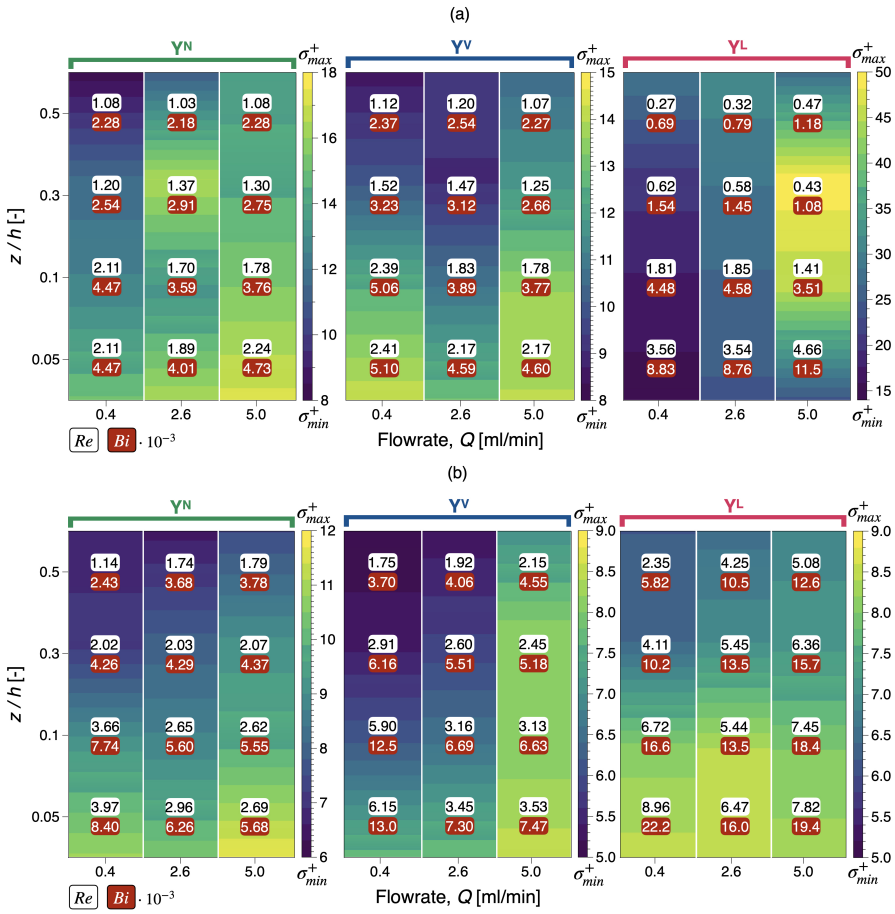

Figure 3.8: Shear stress maps for (a) unstirred and (b) stirred yogurt samples.

resists deformation due to the imposed stress, resulting in stress accumulation and consequently an increase in the shear stress measured. This is especially highlighted in the case of Y^L, which has a large difference between the ramp up and ramp down flow curves in hysteresis loop test due to its higher thixotropy as compared to Y^N and Y^V. The stresses also seem to decrease when we move towards the core of the channel, which is expected as the shear rates are higher near the channel wall and the fluid structure experiences higher

wall friction. Re decreases away from the wall as the viscous forces dominate over inertial forces due to an increase in viscosity near the core, resulting in a plugged flow profile. The decrease in Re is much more significant for Y^L due to dominant viscous effects resulting from high thixotropy of the sample. Similarly, Bi also decreases with depth as the viscous forces and viscoplastic effects compete and the higher viscosity near the core dominates over the yield stress of the sample. More in depth analysis of the velocity profiles of yogurt, Carbopol and Laponite and their stress maps can be found in paper II.

CHAPTER 4

Concluding Remarks and Future Work

4.1 Concluding remarks

Complex fluids are widely used in industrial settings. Understanding their rheological material response is the key to their improved production, processing and prediction of their flow behaviour. In the first paper, rheological characterization of stirred yogurts was performed and their viscoelastic, yield stress and thixotropic material behaviours were studied. The thixotropic material response was then predicted in MITT tests using phenomenological thixotropic models, the parameters of which are determined by fitting the models to hysteresis loop tests. The results show that even when fitting and predicting simple shear flows, careful consideration has to be given to the particular choice of model. Each model captured certain features of yogurt thixotropic test flows while missing others. Thus, modeling and predicting thixotropic data between simple shear flows could be a simple way for evaluating the suitability of thixotropic models for the flow of a particular type of yogurt and, by extension, of other thixotropic fluids. This could have significant implications especially for modeling the flow of yogurts in complex geometries where thixotropy plays a crucial role and there is a need to couple

the flow equations to adequate rheological constitutive models.

In the second paper, flow visualization of 3 different samples of yogurt, Carbopol and Laponite each was performed for the first time using Doppler optical coherence tomography (D-OCT) method. The types/concentrations chosen were motivated by the difference in their rheological properties. Based on their rheological material response, and the imposed flow rate, some samples exhibit a higher plugged profile near the channel surface than the others. As a general rule, velocity profiles get more plugged at lower flow rates for thixotropic samples as the longer travel time of the fluid promotes higher structural recovery. An ex-situ rheometric technique was proposed to construct shear stress distribution maps and Reynolds and Bingham numbers at different depths were highlighted. The stress maps revealed that the stress distribution is greatly affected by the structural state of the material. The shear stress for less structured stirred samples were found to be lower than the unstirred samples. The flow field and stress distribution could have significant implications for modeling the flow of TEVP fluids in milifluidic channels.

4.2 Future Work

As mentioned briefly earlier, the work done in this thesis will be carried forward in the upcoming months and results obtained will be used to perform numerical simulations.

- The constitutive equations used for numerical modeling performed in the first paper will be implemented in a commercial CFD package for simulating flow in pipes, surfaces and microchannels. Based on the performance of the simulation predictions, the constitutive models might be modified to add more physics in terms of yield stress and viscoelasticity.
- Experimental results obtained from D-OCT visualization will be used to validate CFD code.
- Measurements will be performed in pipe flow and surface flow with one or multiple complex fluids considered in this study.
- Microstructural characterizations will be performed and used to estimate the value of structural parameter.

References

[1] R. G. Larson, *The structure and rheology of complex fluids*. Oxford university press New York, 1999, vol. 150.

[2] N. Coleman, "A derivation of the navier-stokes equations," 2010.

[3] J. M. Krishnan, A. P. Deshpande, and P. S. Kumar, *Rheology of complex fluids*. Springer, 2010.

[4] J. San Lee, B. M. Weon, and J. H. Je, "X-ray phase-contrast imaging of dynamics of complex fluids," *Journal of Physics D: Applied Physics*, vol. 46, no. 49, p. 494 006, 2013.

[5] S. M. Al-Zahrani, "A generalized rheological model for shear thinning fluids," *Journal of Petroleum Science and Engineering*, vol. 17, no. 3-4, pp. 211–215, 1997.

[6] H. A. Barnes, J. F. Hutton, and K. Walters, *An introduction to rheology*. Elsevier, 1989, vol. 3.

[7] A. Jaishankar and G. H. McKinley, "Power-law rheology in the bulk and at the interface: Quasi-properties and fractional constitutive equations," *Proceedings of the Royal Society A: Mathematical, Physical and Engineering Sciences*, vol. 469, no. 2149, p. 20 120 284, 2013.

[8] T. Osswald and N. Rudolph, "Polymer rheology," *Carl Hanser, München*, 2015.

[9] S. S. Shibeshi and W. E. Collins, "The rheology of blood flow in a branched arterial system," *Applied Rheology*, vol. 15, no. 6, pp. 398–405, 2005.

[10] M. T. Shaw and W. J. MacKnight, *Introduction to polymer viscoelasticity*. John Wiley & Sons, 2018.

[11] M. Dinkgreve, J. Paredes, M. M. Denn, and D. Bonn, "On different ways of measuring "the" yield stress," *Journal of non-Newtonian fluid mechanics*, vol. 238, pp. 233–241, 2016.

[12] A. Shakeel, A. Kirichek, and C. Chassagne, "Yield stress measurements of mud sediments using different rheological methods and geometries: An evidence of two-step yielding," *Marine Geology*, vol. 427, p. 106 247, 2020.

[13] P. Coussot, Q. D. Nguyen, H. Huynh, and D. Bonn, "Avalanche behavior in yield stress fluids," *Physical review letters*, vol. 88, no. 17, p. 175 501, 2002.

[14] D. C. Cheng, "Yield stress: A time-dependent property and how to measure it," *Rheologica Acta*, vol. 25, pp. 542–554, 1986.

[15] K. te Nijenhuis, G. H. McKinley, S. Spiegelberg, *et al.*, "Springer handbook of experimental fluid mechanics," in C. Tropea, A. L. Yarin, J. F. Foss, *et al.*, Eds. Springer, 2007, ch. 9. Non-Newtonian Flows, pp. 619–732.

[16] M. Fazilati, S. Ingelsten, S. Wojno, T. Nypelö, and R. Kádár, "Thixotropy of cellulose nanocrystal suspensions," *Journal of Rheology*, vol. 65, no. 5, pp. 1035–1052, 2021.

[17] F. J. Stadler, S. Cui, S. Hashmi, *et al.*, "Multiple interval thixotropic test (mitt)—an advanced tool for the rheological characterization of emulsions and other colloidal systems," *Rheologica Acta*, vol. 61, no. 3, pp. 229–242, 2022.

[18] J. N. Miquelim and S. C. Da Silva Lannes, "Egg albumin and guar gum influence on foam thixotropy," *Journal of texture studies*, vol. 40, no. 5, pp. 623–636, 2009.

[19] J. Mewis and N. J. Wagner, "Thixotropy," *Advances in colloid and interface science*, vol. 147, pp. 214–227, 2009.

[20] P. C. Møller, J. Mewis, and D. Bonn, "Yield stress and thixotropy: On the difficulty of measuring yield stresses in practice," *Soft matter*, vol. 2, no. 4, pp. 274–283, 2006.

[21] S. Sharma, V. Shankar, and Y. M. Joshi, "Viscoelasticity and rheological hysteresis," *Journal of Rheology*, vol. 67, no. 1, pp. 139–155, 2023.

[22] G. J. Donley, P. K. Singh, A. Shetty, and S. A. Rogers, "Elucidating the g overshoot in soft materials with a yield transition via a time-resolved experimental strain decomposition," *Proceedings of the National Academy of Sciences*, vol. 117, no. 36, pp. 21 945–21 952, 2020.

[23] A. C. Barbati, J. Desroches, A. Robisson, and G. H. McKinley, "Complex fluids and hydraulic fracturing," *Annual review of chemical and biomolecular engineering*, vol. 7, pp. 415–453, 2016.

[24] T. Benezech and J. F. Maingonnat, "Characterization of the rheological properties of yoghurt—a review," *Journal of Food Engineering*, vol. 21, no. 4, pp. 447–472, 1994.

[25] H. Ramaswamy and S. Basak, "Rheology of stirred yogurts," *Journal of Texture studies*, vol. 22, no. 2, pp. 231–241, 1991.

[26] D. M. Prajapati, N. M. Shrigod, R. J. Prajapati, and P. D. Pandit, "Textural and rheological properties of yoghurt: A review," *Adv Life Sci*, vol. 5, no. 13, pp. 5238–5254, 2016.

[27] H. O'Donnell and F. Butler, "Time-dependent viscosity of stirred yogurt. part i: Couette flow," *Journal of food engineering*, vol. 51, no. 3, pp. 249–254, 2002.

[28] A. Muhammad, "Approaches for improving the rheological characterization of fermented dairy products," 2020.

[29] A. Mujumdar, A. N. Beris, and A. B. Metzner, "Transient phenomena in thixotropic systems," *Journal of Non-Newtonian Fluid Mechanics*, vol. 102, no. 2, pp. 157–178, 2002.

[30] J. Pearson and P. Tardy, "Models for flow of non-newtonian and complex fluids through porous media," *Journal of Non-Newtonian Fluid Mechanics*, vol. 102, no. 2, pp. 447–473, 2002.

[31] A. Hassan, R. Ipsen, T. Janzen, and K. Qvist, "Microstructure and rheology of yogurt made with cultures differing only in their ability to produce exopolysaccharides," *Journal of dairy science*, vol. 86, no. 5, pp. 1632–1638, 2003.

[32] T. Paseephol, D. M. Small, and F. Sherkat, "Rheology and texture of set yogurt as affected by inulin addition," *Journal of Texture Studies*, vol. 39, no. 6, pp. 617–634, 2008.

[33] S. Curran, R. Hayes, A. Afacan, M. Williams, and P. Tanguy, "Properties of carbopol solutions as models for yield-stress fluids," *Journal of food science*, vol. 67, no. 1, pp. 176–180, 2002.

[34] M. Dinkgreve, M. Fazilati, M. Denn, and D. Bonn, "Carbopol: From a simple to a thixotropic yield stress fluid," *Journal of Rheology*, vol. 62, no. 3, pp. 773–780, 2018.

[35] Y. M. Joshi, G. R. K. Reddy, A. L. Kulkarni, N. Kumar, and R. P. Chhabra, "Rheological behaviour of aqueous suspensions of laponite: New insights into the ageing phenomena," *Proceedings of the Royal Society A: Mathematical, Physical and Engineering Sciences*, vol. 464, no. 2090, pp. 469–489, 2008.

[36] W. Worrall and S. Tuliani, "Viscosity changes during the ageing of clay-water suspensions," *Trans Brit Ceramic Soc*, vol. 63, pp. 167–185, 1964.

[37] L. Schmitt, G. Ghnassia, J. Bimbenet, and G. Cuvelier, "Flow properties of stirred yogurt: Calculation of the pressure drop for a thixotropic fluid," *Journal of Food Engineering*, vol. 37, no. 4, pp. 367–388, 1998.

[38] A. G. Podoleanu, "Optical coherence tomography," *Journal of microscopy*, vol. 247, no. 3, pp. 209–219, 2012.

[39] D. Huang, E. A. Swanson, C. P. Lin, *et al.*, "Optical coherence tomography," *science*, vol. 254, no. 5035, pp. 1178–1181, 1991.